ACS OMEGA

http://pubs.acs.org/journal/acsodf

Article

Gold-Nanoparticles-Enhanced Production of Reactive Oxygen Species in Cells at Spread-Out Bragg Peak under Proton Beam Radiation

Chang-Yun Lo, Shiao-Wen Tsai, Huan Niu, Fang-Hsin Chen, Hsiao-Chien Hwang, Tsi-Chian Chao, Ing-Tsung Hsiao, and Jiunn-Woei Liaw*

Cite This: *ACS Omega* 2023, 8, 17922−17931

Read Online

ACCESS | Metrics & More | Article Recommendations | Supporting Information

ABSTRACT: This study investigates the radiobiological effects of gold nanoparticles (GNPs) as radiosensitizers for proton beam therapy (PBT). Specifically, we explore the enhanced production of reactive oxygen species (ROS) in GNP-loaded tumor cells irradiated by a 230 MeV proton beam in a spread-out Bragg peak (SOBP) zone obtained by a passive scattering system. Our findings indicate that the radiosensitization enhancement factor is 1.24 at 30% cell survival fraction, 8 days after 6 Gy proton beam irradiation. Since protons deposit the majority of their energy at the SOBP region and interact with GNPs to induce more ejected electrons from the high-Z GNPs, these ejected electrons then react with water molecules to produce excessive ROS that can damage cellular organelles. Laser scanning confocal microscopy reveals the excessive ROS induced inside the GNP-loaded cells immediately after proton irradiation. Furthermore, the damage to cytoskeletons and mitochondrial dysfunction in GNP-loaded cells caused by the induced ROS becomes significantly severe, 48 h after proton irradiation. Our biological evidence suggests that the cytotoxicity of GNP-enhanced ROS production has the potential to increase the tumoricidal efficacy of PBT.

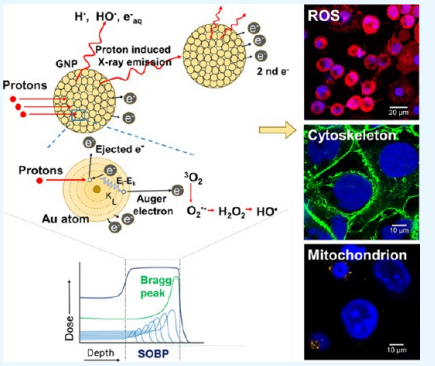

INTRODUCTION

Proton beam therapy (PBT) is a prospective modality of cancer treatment.[1−3] Several studies have shown that the relative biological effectiveness (RBE) of PBT is superior to photon therapy, e.g., X-ray.[4−8] An important feature of proton therapy is that the slow-down protons deposit most energy at the end of the path in tissues to generate severe damage. The curve of the spatial energy distribution of protons indicates that the deposition culminates within a narrow region, which is called the Bragg peak (BP).[9−17] This is to say that the radiobiological cytotoxicity of PBT mainly occurs at the BP zone. Based on this feature, the PBT can perform a selective-area treatment of tumors with less damage on the other normal tissue in the path of the proton beam. In contrast, the photon therapy always causes the most severe damage on the tissue at the beginning of the path. Similar to the other radiotherapies, PBT not only induces the single-strand break (SSB) and double-strand break (DSB) of DNA directly but also induces an excessive production of reactive oxygen species (ROS), which has a longer lifetime to induce the damage of DNA subsequently.[18−24] Since the depth of BP is very thin, a proton beam normally needs to pass through certain scattering devices to produce a spread-out Bragg peak (SOBP) zone, which covers a larger area with a uniform dose for the practical applications.[25−31]

Recently, a lot of research has shown that gold nanoparticles (GNPs) can enhance the production of ROS during the radiotherapy.[14,32−43] The deposited protons collide with GNPs at the BP zone to induce more ejected electrons from high-Z GNPs.[14,44] These high-energy protons induce secondary electrons, photons (e.g., X-rays or gamma emission), and positrons from GNPs via a low linear energy transfer.[14,45,46] And then the secondary electrons interacting with water molecules generate excessive amounts of ROS. In particular, the production of hydroxyl radicals ($^{\bullet}OH$) and superoxide anions ($O_2^{\bullet-}$) is enhanced by the interaction of GNPs with proton beam.[14] The excessive ROS may damage cellular DNA and organelles to induce apoptosis.[47,48] Through the pathway of producing excessive amount of ROS, GNPs may raise the efficacy of PBT.[49] In addition, a lot of research has demonstrated the feasibility of using GNP to enhance the efficacy of PBT based on the Monte Carlo simulation.[50−61] On the other hand, the direct damage of GNP-enhanced PBT on

Received: February 15, 2023
Accepted: April 26, 2023
Published: May 9, 2023

DNA is seemed to be insignificant, according to the simulation of ref 62. This implies that the other pathway might be contributed by the radiosensitization effect of GNPs, e.g., ROS. Since the lifetime and the mean-free path of the induced ROS are longer than those of the ejected electrons, we infer that the excessive ROS induced by GNPs in the cytoplasm may play a critical role on cell damage. Several studies further showed that via GNPs to raise the ROS level in cancer cells might be a prospective pathway to damaging tumor and inhibiting the DNA repair.[63,64] However, there is a lack of direct biological evidence in the excessive production of ROS in cells and the related cellular organelles' damage caused by GNPs interplaying with proton beam. In the previous research study, we have studied the function of GNPs for enhancing the production of ROS in tumor cells and then inducing the follow-up damage on the cytoskeleton as being irradiated by a two-photon laser (femtosecond laser) and Cs-137.[65,66] We think the mechanism is that as GNPs are irradiated by two-photon pulses or Cs-137, a certain number of energetic hot electrons or secondary electrons are scattered to escape from the GNPs and then interact with the water molecules in their proximity. Consequently, the excessive ROS is produced in cells with the assistance of GNPs as irradiated by a two-photon laser or Cs-137, compared to the control without GNPs.[65,66] For both cases, the excessive ROS on cell's damage, e.g., cytoskeletons, were verified. In addition, if an antioxidant, e.g., *N*-acetyl-L-cysteine, or ROS scavenger, e.g., dimethyl sulfoxide, is added in these GNP-loaded cells, the cell's damage is reduced and the survival fraction (SF) is raised after the irradiation of a two-photon laser or proton beam.[66,67] These results imply that the excessive ROS produced by GNPs interacting the incident photons or protons is the critical factor to induce the cellular apoptosis.

In this paper, the energy of the proton beam is 230 MeV. The radiobiological effect of GNPs on cells as being irradiated by the proton beam at the SOBP zone is studied. Two passive scattering systems, one for a horizontal beam and the other for a vertical beam, were used to induce the SOBP zone in experiments. The study aims to identify the radiosensitization enhancement factor (REF) resulting from the interaction between GNPs and the proton beam.[32,41,66] Additionally, we quantitatively analyze the amount of reactive oxygen species (ROS) in GNP-loaded cells from images obtained by laser scanning confocal microscopy (LSCM), and qualitatively investigate the damage to cellular organelles from LSCM images. The findings of this study may contribute to the development of GNP-enhanced PBT.

METHODS AND SYSTEMS

Physical Experiments. All experiments of proton irradiation were conducted in Chang Gung Memorial Hospital in Linkou. A proton therapy system, including a cyclotron, was used for biological experiments, manufactured by Sumitomo Heavy Industries, Ltd., Japan. In order to produce an effect of SOBP, two passive scattering systems were utilized for the horizontal and vertical radiation configurations, as shown in Figure 1A,B. The former is for the experiments of clonogenic assay, and the latter is for the experiments of cellular organelles' damage assay. There are several components in the two configurations to adjust the SOBP zone for experiments. In the passive scattering system of the horizontal beam, a double-scattering device with a collimator was designed and setup by our group, as shown in Figure 1A.

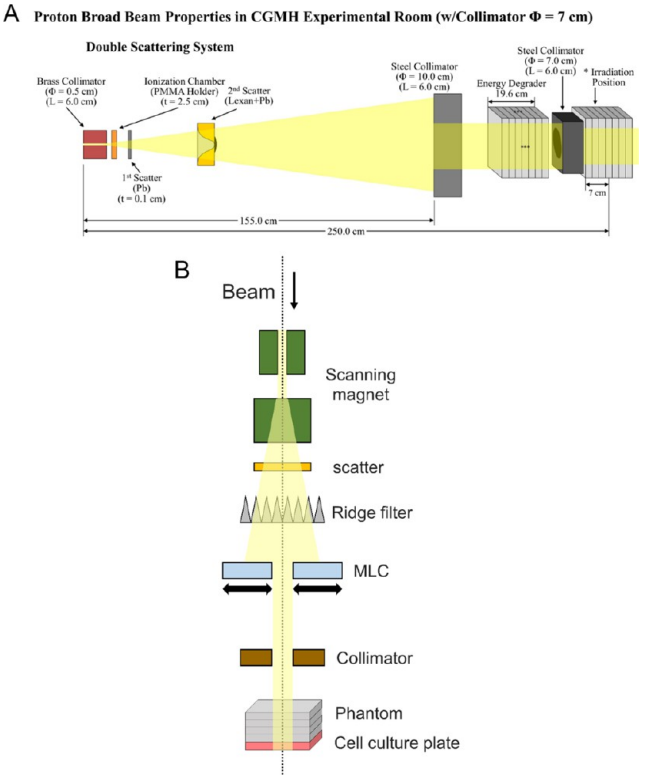

Figure 1. Two passive scattering systems for horizontal and vertical proton beams. (A) Horizontal configuration with double scattering devices. Sample tubes are placed inside the phantom at a position in the SOBP zone. (B) Vertical configuration with a ridge filter and a tungsten MLC. Cell culture plate is placed under the phantom at a position in the SOBP zone.

The first scatterer is a Pb plate of 1 mm, and the second one is a Lexan with a Pb cup. A brass collimator with a PMMA holder and two steel collimators. Two phantoms made of high-density polyethylene (HDPE) for the energy degrader and holder of the sample are used. The HDPE is a water-equivalence plastic material, which can simulate the tissue. The diameter of the beam profile is about 5 cm with 95% energy at the sample location. The width of the SOBP range in HDPE is 61.3 mm; an equivalent depth in water is 27 cm. Samples are placed within the SOBP zone of the proton beam inside the last phantom. Another passive scattering system for the vertical beam was provided by Sumitomo Heavy Industries, as shown in Figure 1B. A wobbling and scattering magnet through a Pb-scatter and a ridge filter to expand a SOBP, and then through a tungsten multi-leaf collimator (MLC), a compensator and collimator to the target, placed in HDPE phantom. The schematic of the dose of proton beam versus the depth in tissue is plotted in Figure 2, where the SOBP zone is the last area of the path of protons depositing their energy. In contrast, the cure of the dose of X-ray decay versus the depth shows a distance decay behavior in tissue. The mechanism of the enhanced production of ROS (e.g., hydroxyl radicals and superoxide anions) through the interaction of protons with GNPs is plotted in Figure 3.[33,49] The slowing-down protons in the SOBP zone interact with gold atoms to release the primary ejected electrons from the lower shell through Coulomb interaction. Subsequently, the proton-induced X-ray or gamma-ray emission accompany due to the electrons of the higher shell to fill the holes in the lower shell. Consequently,

https://doi.org/10.1021/acsomega.3c01025
ACS Omega 2023, 8, 17922−17931

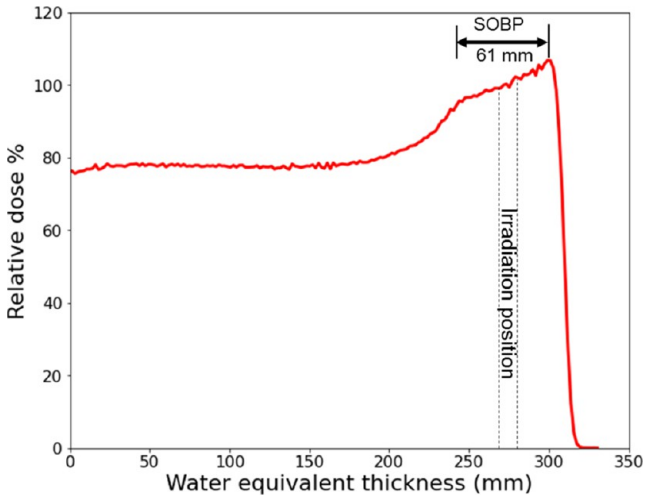

Figure 2. Measured dose of the proton beam versus the water equivalent depth for the passive scattering system, as shown in Figure 1A. The length of the SOBP zone is 6.13 cm.

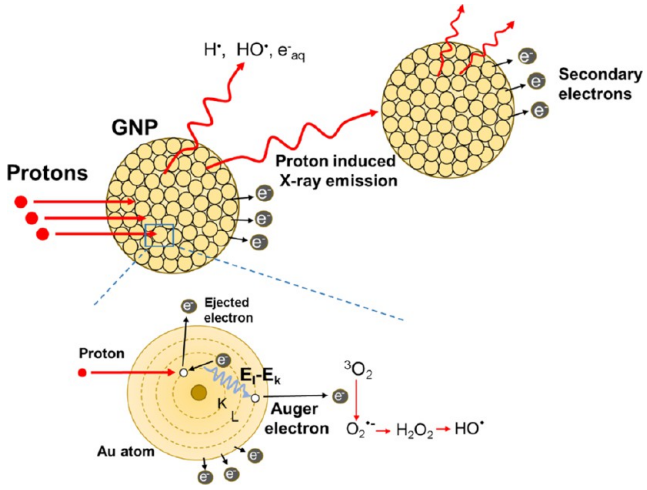

Figure 3. Mechanism of producing ROS through the incident protons interacting with gold atoms in a GNP to release the primary ejected electrons, X-ray emission, and Auger electrons. Subsequently, all these primary and secondary ejected electrons may react with the surrounding water molecules to generate ROS, such as hydroxyl radicals ($^{\bullet}OH$) and superoxide anions ($O_2^{\bullet-}$).

Auger electrons could also be emitted from the atoms from the subsequent de-excitation process. In addition, the proton-induced X-rays and the ejected electrons from an atom may interact with the other nearby atoms so as to release more secondary electrons. Therefore, all these primary and secondary ejected electrons from GNPs may react with the surrounding water molecules to generate ROS, particularly in the SOBP zone of the proton beam.

BIOLOGICAL EXPERIMENT

The GNPs we used were synthesized with an average size of 55 nm, according to the protocol.[65,66] Cell line of A431, human epidermoid carcinoma, was used for the experiment. The cell line of A431 was purchased from the Food Industry Research and Development Institute in Taiwan. Culture tubes with GNP-loaded cell suspension, placed in a HDPE phantom at the SOBP region, were irradiated by a horizontal proton beam, as shown in Figures 1A and 2. After the proton beam irradiation, these cells were moved to dishes for the clonogenic assay to quantify the reproductive cell survival. Dulbecco's modified eagle's complete medium (4.5 g/l D-glucose, Gibco by Life Technologies, MA, USA) was used for cell culture (Figure 4).

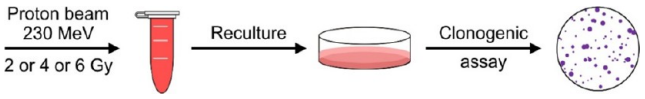

Figure 4. Cell suspension tubes (control and 80 ppm GNP-supplemented samples) are placed in a HDPE phantom in the SOBP region for the radiation of a horizontal proton beam at different doses. Proton-treated cells were immediately cultured on dishes and incubated for 8 days at 37 °C. And then, the survival fractions of the clonogenic assay were measured.

In addition, the vertical proton beam was used to irradiate cells incubated in well plate for the measurement of the extra ROS and organelles' damages in cells. Different fluorescence kits were used to detect ROS and specific organelles. We used LSCM (ZEISS LSM 780 META) to acquire the cellular images. Specific laser for exciting the specific fluorescence kit and the corresponding band-pass filter for detecting the emission of these fluorescent lights are set for LSCM images. The LSCM images are acquired point by point under the excitation of focused lasers. The fluorescence intensities of different kits are detected individually by a highly sensitive photomultiplier tube (PMT) via the corresponding filter. The PMT can only detect the intensity of photons but cannot distinguish the color of fluorescence. Therefore, a specific bandpass filter is needed for the detection of the fluorescence. For example, the kit for labeling ROS is Carboxy-H_2DCFDA; the exciting wavelength of the laser is 488 nm, and the range of the corresponding band-pass filter is [509, 535] nm.[66] The carboxy-H_2DCFDA is originally nonfluorescent. It can be converted to carboxy-DCFH when the acetate groups are removed by intracellular esterases (enzymes) in cells. Once there is any ROS generated in the cell, carboxy-DCFH immediately becomes a green-fluorescent carboxy-DCF due to the oxidation caused by the activity of ROS. This fluorophore (carboxy-DCF) can remain active in cells for several hours. Therefore, there is sufficient time for us to detect ROS via this fluorophore by LSCM. Although the lifetime of ROS is short, the active time of carboxy-DCF is long enough for measurement. Normally, we can complete the measurement of ROS within 1 h right after the proton irradiation. Actually, the fluorescence of carboxy-DCF is green in color. Herein, a red pseudocolor is used to visualize ROS. The kit for labeling cytoskeletons is Alexa Fluor 488 Phalloidin; the exciting wavelength of the laser is 488 nm, and the range of the band-pass filter is [500, 553] nm. The kit for labeling mitochondria is MitoCapture; the exciting wavelength of the laser is 488 nm, and the range of the band-pass filter is [580, 598] nm. The kit for labeling nuclei is Hoechst 33342; the exciting wavelength of the laser is 405 nm, and the range of the band-pass filter is [410, 472] nm. In order to distinguish different fluorescence expressions, different pseudocolors are used in these LSCM images; these fluorescence colors depicted in the LSCM images throughout this paper are not the true colors. For example, we use red for ROS, blue for nuclei, green for cytoskeletons, and yellow for mitochondria, respectively.

https://doi.org/10.1021/acsomega.3c01025
ACS Omega 2023, 8, 17922−17931

RESULTS AND DISCUSSION

The cells of A431 were co-cultivated with a medium containing 80 ppm GNPs for 24 h prior. The cell image of transmission

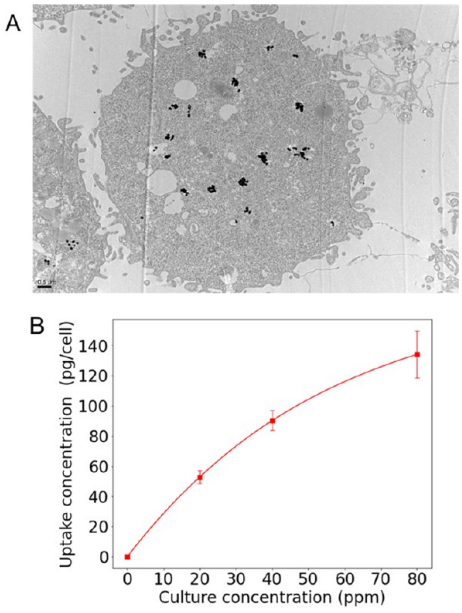

Figure 5. (A) TEM image of a GNP-loaded cell (A431) through endocytosis. Different numbers of GNPs (black dots) accumulated in several vesicles in the cytoplasm. The scalar bar is 500 nm. (B) Amount of GNPs uptake per cell after 24 h co-culture versus the concentration of GNPs in the culture medium.

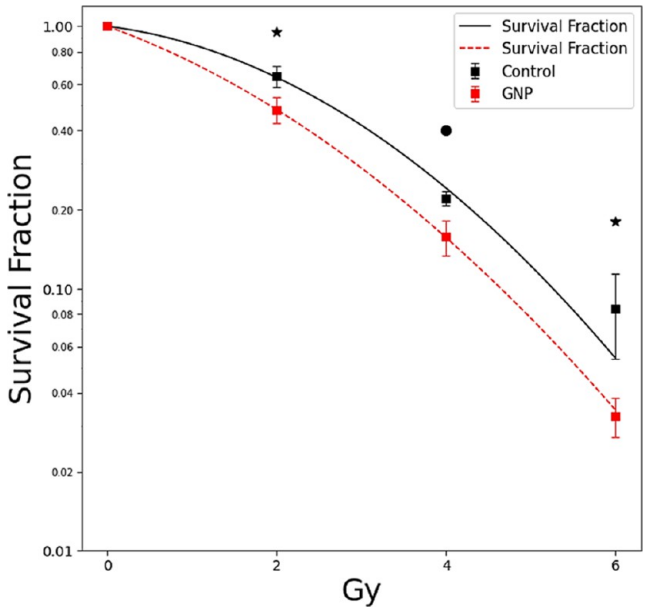

Figure 6. Cell viability (in vitro clonogenic assay) for A431 cells with GNP uptake. Cell survival fraction, 8 days after 230 MeV proton radiation, versus radiation dose. Control group: cells without GNP treatment. $^{\star}p < 0.05$, $^{\bullet}p < 0.02$.

electron microscopy (TEM) is shown in Figure 5A; it indicates that a certain number of GNPs are accumulated in several vesicles in the cytoplasm through the endocytosis and the vesicles' fusion. Figure 5B shows the amount of GNP uptake per cell in different concentrations of GNPs in the culture

Table 1. AFs and REF of GNPs on the Cell SF Irradiated by 230 MeV Proton Beam, Calculated from Cell's SF Versus Radiation Dose

	AF (2 Gy)	AF (4 Gy)	AF (6 Gy)	REF at 30%
230 MeV Proton	17.60%	23.49%	33.99%	1.238

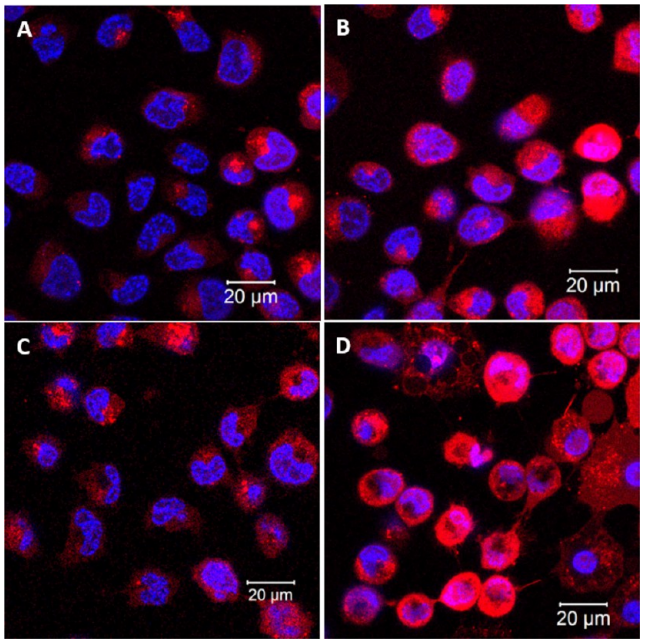

Figure 7. Cell fluorescence images (magnification of 63×) of labeled ROS (pseudocolor of red) under LSCM, right after 6 Gy proton beam irradiation. (A,B) Images of the controls before and after the proton beam irradiation, respectively. (C,D) Images of the GNP-loaded cells before and after the proton beam irradiation, respectively. Blue indicates the nuclei.

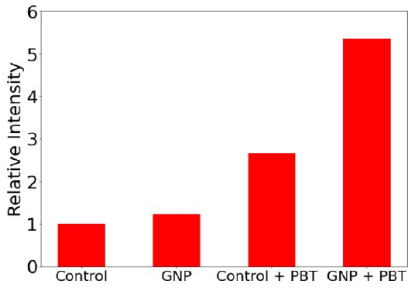

Figure 8. Average relative intensities of ROS per cell for four groups; controls, GNP-loaded cells, and controls as well as GNP-loaded cells irradiated by a 6 Gy proton beam at SOBP.

medium after 24 h co-culture. In general, a higher concentration of the medium tends to result in a greater amount of uptake. However, it seems that the amount of GNP internalized by cells tends to saturate. For example, the average amount of GNP uptake per cell after 24 h is about 134 picograms for 80 ppm medium after 24 h co-culture.[68] Subsequently, we studied the radiobiological effect of GNPs irradiated by proton beam on the cell survival, as shown in Figure 6. The clonogenic assay method was used to measure the viability of cells, 8 days after proton irradiation of different doses (0, 2, 4, and 6 Gy), where the horizontal beam was used. Figure 6 shows the curves of SFs for the GNP-loaded cells and the control (without GNP treatment) versus the proton dose.

https://doi.org/10.1021/acsomega.3c01025
ACS Omega 2023, 8, 17922−17931

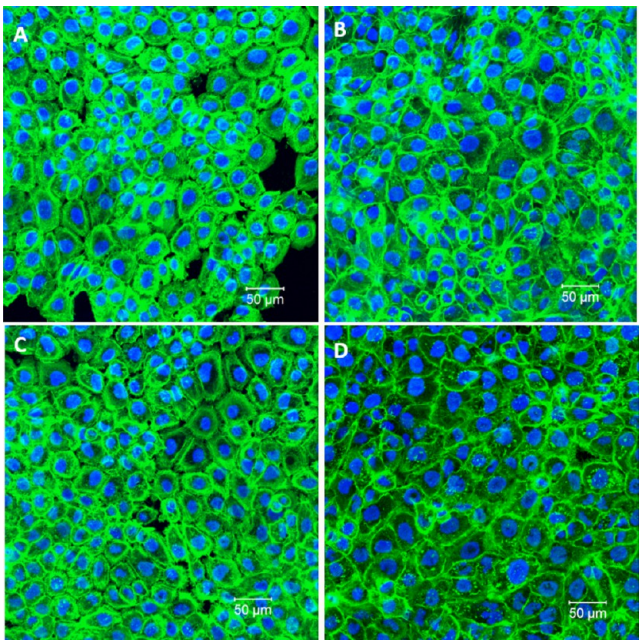

Figure 9. Cell fluorescence images (magnification of 20×) of labeled cytoskeletons (pseudocolor of green) under LSCM, 24 h after 6 Gy proton beam irradiation. (A,B) Images of the controls without and with the proton beam irradiation, respectively. (C,D) Images of the GNP-loaded cells without and with the proton beam irradiation, respectively.

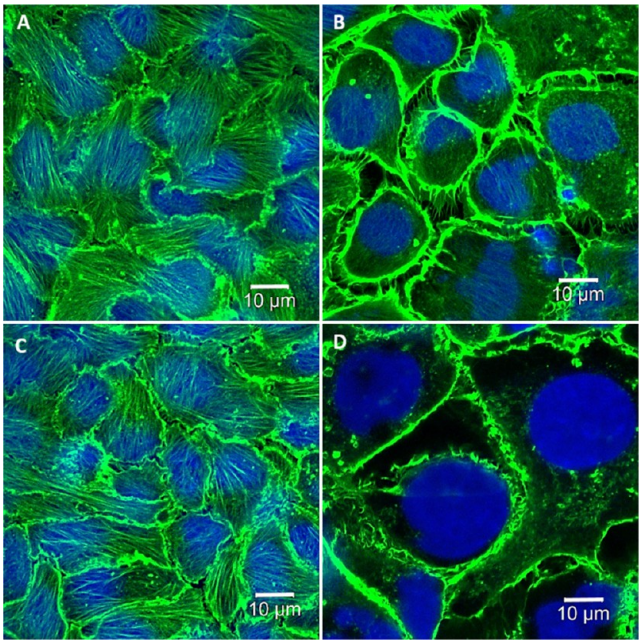

Figure 10. Cell fluorescence images (magnification of 100×) of labeled cytoskeletons (pseudocolor of green) under LSCM, 48 h after 6 Gy proton beam irradiation. (A,B) Images of the controls without and with the proton beam irradiation, respectively. (C,D) Images of the GNP-loaded cells without and with the proton beam irradiation, respectively.

Here, an exponential decay model for SF in terms of linear and quadratic forms of the dose D is used for curve fitting, which is expressed by

$$\mathrm{SF} = \mathrm{e}^{-(\alpha D+\beta D^2)} \tag{1}$$

where α and β are the inactivation constants. From the two curves, the REF of GNPs on proton irradiation is defined as the ratio of the dose without GNPs to the dose with GNPs at 30% SF; REF is 1.24[32,41,66]

$$\mathrm{REF} = \frac{D(\text{without GNPs}) \text{ at } 30\% \text{ SF}}{D(\text{with GNPs}) \text{ at } 30\% \text{ SF}} \tag{2}$$

In addition, the amplification factor (AF) of GNP on cell SF at a specific dose is defined as the ratio of SF difference

$$\mathrm{AF} = \frac{\mathrm{SF}_{\mathrm{control}} - \mathrm{SF}_{\mathrm{with\ GNPs}}}{\mathrm{SF}_{\mathrm{control}}} \times 100\% \tag{3}$$

The AFs at different doses and the REF are listed in Table 1. These results provide quantitative evidence that GNPs have the potential to enhance the RBE of PBT as radiosensitizers.

Moreover, these GNP-loaded cells were irradiated by a 6 Gy proton beam at the SOBP zone by a vertical beam, as shown in Figure 1B. The fluorescence expression of the kit (carboxy-H_2DCFDA) for labeling ROS in these cells and the controls was measured by LSCM right after the irradiation. In fact, the fluorescence of this kit is green in color. Herein, a red pseudocolor is used to visualize ROS, as shown in Figure 7. Figure 7 shows these images (magnification of 63×) of four groups (control, GNP-loaded cell, and both irradiated by a 6 Gy proton beam at SOBP), where the red pseudocolor represents the ROS expression and the blue color represents the nucleus. The other images (magnification of 20×) are shown in Figure S1 (Supporting Information). These results indicate that the ROS amount of the GNP-loaded cells irradiated by the proton beam at the SOBP zone is obviously stronger than that of the control. The elevated ROS level in these cells could be induced by the Coulomb-ejected electrons and Auger electrons released from GNPs interacting with the deposited protons in the SOBP zone. In addition, the necrosis of several GNP-loaded cells caused by the excessive ROS can be observed in Figure 7D, the loss of membrane integrity (the swelling). There are two filters set for LSCM to collect the different fluorescence intensities of the ROS kit and the nucleus kit individually by a PMT. In order to distinct both fluorescence expressions, two pseudocolors are used in these LSCM images to show the ROS (red) and nucleus (blue) individually. Notice that these fluorescence colors in these images of LSCM are pseudocolors rather than true colors. In fact, the fluorescence color of the ROS kit is green. Moreover, the average relative intensities of ROS per cell of Figure S1 (magnification of 20×) were analyzed by Image J, as shown in Figure 8. For the each group, three images (magnification of 20×) at different sites were acquired individually and then processed by Image J to obtain the average intensity of ROS per cell; the number of cells is more than 350 for each group. Moreover, we normalized these values by those of the control to obtain the average relative intensities, as shown in Figure 8. Obviously, after the 6 Gy proton irradiation, the average relative intensity of ROS in these GNP-loaded cells is higher than that in those cells without GNPs. The quantitative comparison between the four groups illustrates that GNPs can enhance the ROS production in cells under the proton irradiation.

Furthermore, we investigated the effect of the excessive ROS induced by GNPs on the damage of organelles. Figure 9 (magnification of 20×) and 10 (magnification of 100×) show the fluorescence expression of the cytoskeletons in cells,

https://doi.org/10.1021/acsomega.3c01025
ACS Omega 2023, 8, 17922−17931

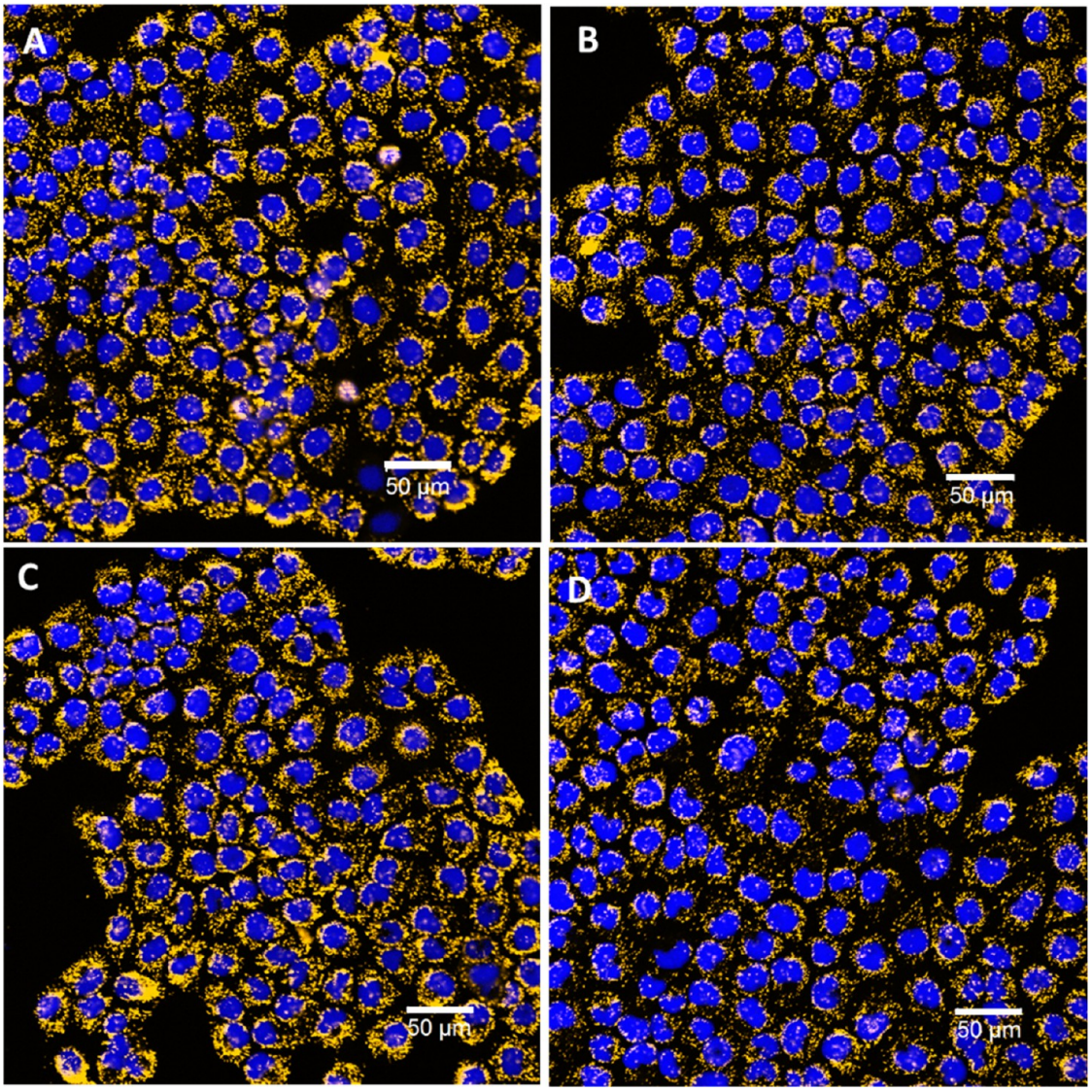

Figure 11. Cell fluorescence images (magnification of 20×) of labeled active mitochondria (pseudocolor of yellow) under LSCM, 6 h after 6 Gy proton beam irradiation. (A,B) Images of the controls without and with the proton beam irradiation, respectively. (C,D) Images of the GNP-loaded cells without and with the proton beam irradiation, respectively.

labeled by Alexa Fluor 488 Phalloidin (green), for 24 and 48 h after the irradiation, respectively. The integrity of the cytoskeletons in the control cells and the GNP-loaded cells are nearly identical prior to proton beam irradiation. After 24 h of exposure to a 6 Gy proton beam, the GNP-loaded cells exhibited more significant cytoskeleton disruptions compared to the control cells. After 48 h, the disruptions to the cytoskeleton in cells loaded with GNPs become significantly more pronounced than in the control group, as shown in Figure 8. The disruptions could be caused by the depolymerization of actin filaments. In addition, the swelling of the nucleus is also observed in these GNP-loaded cells irradiated by a proton beam. The cell images (magnification of 20×) of labeled cytoskeletons at different times (1, 6, 48, and 72 h) are shown in Figures S2−S5 (Supporting Information), respectively (Figure 10).

The LSCM images in Figure 11 (magnification of 20×) and Figure 12 (magnification of 100×) depict the fluorescence expression of active mitochondria labeled by MitoCapture, taken 6 and 48 h after 6 Gy irradiation, respectively. The yellow spots in the cells represent the MitoCapture fluorescence. Comparing the results, a significant reduction in active mitochondrial expression caused by the irradiation is evident. Furthermore, the difference in mitochondrial damage between GNP-loaded cells and controls becomes significant after 6 h, as shown in Figure 11. After 48 h, there is nearly no activate mitochondria in these GNP-loaded cells compared to the controls without GNPs, as shown in Figure 12. In addition, the cell images (magnification of 20×) of active mitochondria at different times (3, 24, 48, and 72 h) after the irradiation are shown in Figures S6−S9 (Supporting Information), respectively. The results indicate that excessive ROS generated by GNPs interacting with proton beam can cause mitochondrial damage. In the early stage of cell damage, the cell will try to repair itself. If, however, the cell damage is too severe, the cell will trigger the apoptosis mechanism. Thus, it may require 24 h to observe significant apoptosis instead of just 1 or 2 h.

In summary, the radiobiological response indicates that the REF of GNPs on PBT at 30% survival fraction is 1.24. Furthermore, the relative amount of ROS in GNP-loaded cells

https://doi.org/10.1021/acsomega.3c01025
ACS Omega 2023, 8, 17922−17931

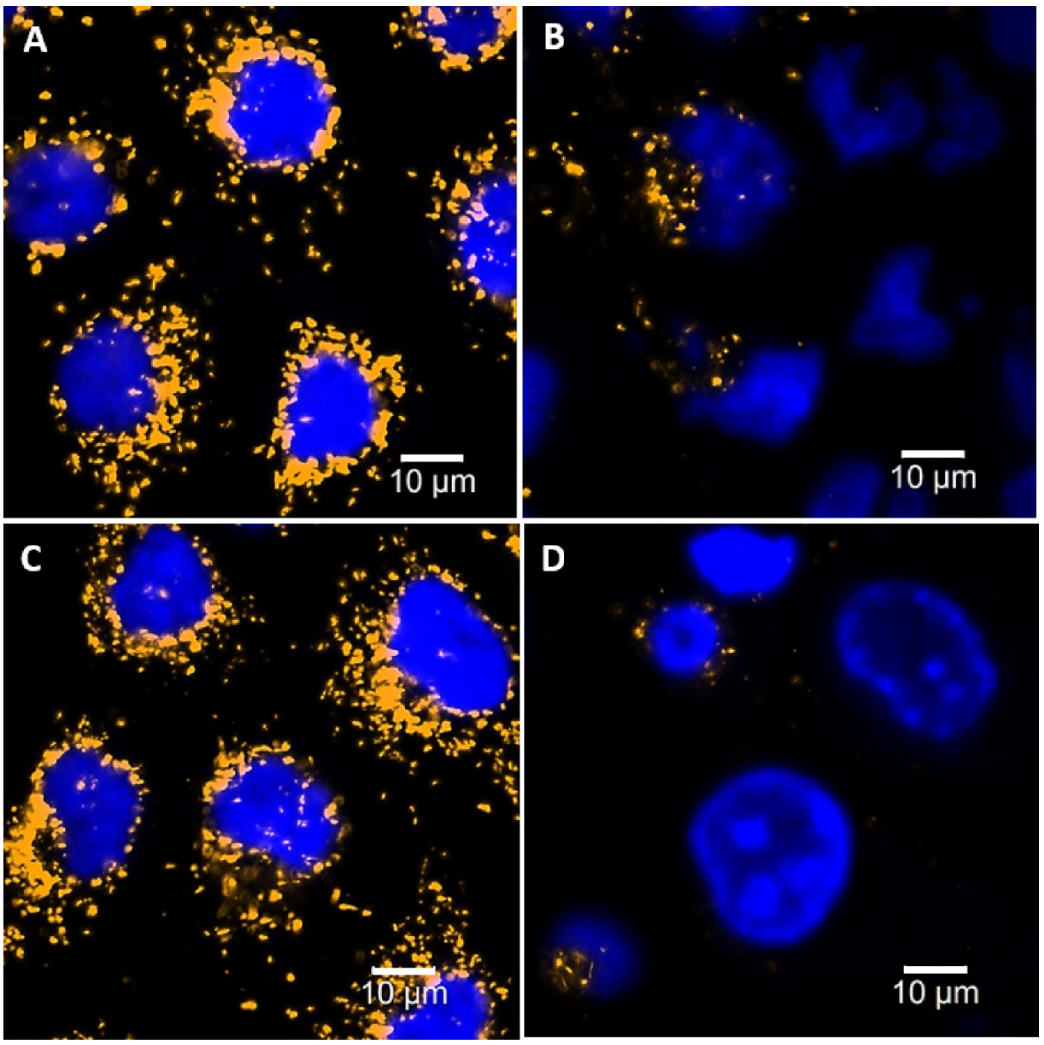

Figure 12. Cell fluorescence images (magnification of 100×) of labeled active mitochondria (pseudocolor of yellow) under LSCM, 48 h after 6 Gy proton beam irradiation. (A,B) Images of the controls without and with the proton beam irradiation, respectively. (C,D) Images of the GNP-loaded cells without and with the proton beam irradiation, respectively.

irradiated by a 230 MeV proton beam at the SOBP zone is significantly higher compared to the controls. The LSCM fluorescence images indicate that disruption of cytoskeletons and dysfunction of mitochondria in GNP-loaded cells irradiated by the proton beam are more pronounced than in the controls. The quantitative REF and qualitative radiobiological evidence demonstrate the potential of using GNPs as radiosensitizers to enhance the RBE of PBT in the SOBP zone.

CONCLUSIONS

This paper presents a study on the radiobiological effects of GNPs as radiosensitizers for PBT in the SOBP zone. Our results demonstrate that GNPs can enhance the tumoricidal efficacy of PBT, with a REF of 1.24 at 30% cell survival fraction 8 days after 6 Gy proton beam irradiation. The mechanism of GNPs as radiosensitizers involves the production of excessive ROS induced by ejected electrons from GNPs interacting with water molecules after proton irradiation. The significant disruption of the cytoskeletons and mitochondrial dysfunction observed in GNP-loaded cells after proton irradiation further supports this mechanism. Our findings suggest that GNPs can be used to increase ROS production and promote apoptosis or necrosis. These results provide a new direction for Monte Carlo simulations and may have implications for improving the effectiveness of PBT.[69,70] In addition, the pathway of inducing high levels of ROS through the interaction of GNPs with a proton beam may be useful in damaging the cellular DNA/mtDNA and organelles of certain radioresistant tumor cells, particularly cancer stem cells.

ASSOCIATED CONTENT

Supporting Information

The Supporting Information is available free of charge at https://pubs.acs.org/doi/10.1021/acsomega.3c01025.

Cell fluorescence images of labeled ROS under LSCM, right after 6 Gy proton beam irradiation; cell fluorescence images of labeled cytoskeletons under LSCM, 1, 6, 48, and 72 h after 6 Gy proton beam irradiation; and cell fluorescence images of labeled mitochondria under LSCM, 3, 24, 48, and 72 h after 6 Gy proton beam irradiation (PDF)

https://doi.org/10.1021/acsomega.3c01025
ACS Omega 2023, 8, 17922−17931

AUTHOR INFORMATION

Corresponding Author

Jiunn-Woei Liaw − *Department of Mechanical Engineering, Chang Gung University, Taoyuan 333, Taiwan; Proton and Radiation Therapy Center, Linkou Chang Gung Memorial Hospital, Taoyuan 333, Taiwan; Department of Mechanical Engineering, Ming Chi University of Technology, New Taipei City 243, Taiwan;* orcid.org/0000-0003-0179-5274; Email: markliaw@mail.cgu.edu.tw

Authors

Chang-Yun Lo − *Department of Mechanical Engineering, Chang Gung University, Taoyuan 333, Taiwan*

Shiao-Wen Tsai − *Department of Biomedical Engineering, Chang Gung University, Taoyuan 333, Taiwan; Department of Periodontics, Chang Gung Memorial Hospital, Taipei 105, Taiwan;* orcid.org/0000-0002-6225-6613

Huan Niu − *Accelerator Laboratory, Nuclear Science and Technology Development Center, National Tsing Hua University, Hsinchu 300, Taiwan*

Fang-Hsin Chen − *Institute of Nuclear Engineering and Science, National Tsing Hua University, Hsinchu 300, Taiwan; Department of Radiation Oncology, Chang Gung Memorial Hospital, Taoyuan 333, Taiwan; Department of Medical Imaging and Radiological Science, Chang Gung University, Taoyuan 333, Taiwan;* Present Address: F.-H.C. current affiliation is Institute of Nuclear Engineering and Science at National Tsing Hua University. The research was conducted during her previous affiliations: Department of Radiation Oncology at Chang Gung Memorial Hospital and Department of Medical Imaging and Radiological Science at Chang Gung University

Hsiao-Chien Hwang − *Proton and Radiation Therapy Center, Linkou Chang Gung Memorial Hospital, Taoyuan 333, Taiwan*

Tsi-Chian Chao − *Department of Medical Imaging and Radiological Science, Chang Gung University, Taoyuan 333, Taiwan*

Ing-Tsung Hsiao − *Department of Medical Imaging and Radiological Science, Chang Gung University, Taoyuan 333, Taiwan*

Complete contact information is available at: https://pubs.acs.org/10.1021/acsomega.3c01025

Author Contributions

C.Y.L., S.W.T., and J.W.L. drafted the manuscript. H.N. designed the horizontal double scattering devices. C.Y.L., F.H.C., H.C.H., T.C.C., and I.T.H. conducted the experiments. J.W.L. coordinated the projects and revised the manuscript. All authors read and approved the final manuscript.

Notes

The authors declare no competing financial interest.

ACKNOWLEDGMENTS

The research was supported by Chang Gung Memorial Hospital (CIRPD2I0021, CIRPD2I0022, and CIRPD2I0023). The authors thank the Microscopy Center at Chang Gung University and the Particle Physics and Beam Delivery Core Laboratory at Chang Gung Memorial Hospital, Linkou for technical assistance.

ABBREVIATIONS

GNPs:gold nanoparticles; SOBP:spread-out Bragg peak; ROS:reactive oxygen species; LSCM:laser scanning confocal microscopy; DSB:double strand break; SSB:single strand break; SF:survival fraction; REF:radiosensitization enhancement factor; AF:amplification factor; TEM:transmission electron microscope; HDPE:high density polyethylene; PBT:proton beam therapy; RBE:relative biological effectiveness; PMT:photomultiplier tube

REFERENCES

(1) Levin, W. P.; Kooy, H.; Loeffler, J. S.; DeLaney, T. F. Proton beam therapy. *Br. J. Cancer* **2005**, *93*, 849−854.

(2) Hiroshima, Y.; Ishikawa, H.; Murakami, M.; Nakamura, M.; Shimizu, S.; Enomoto, T.; Oda, T.; Mizumoto, M.; Nakai, K.; Okumura, T.; Sakurai, H. Proton beam therapy for local recurrence of rectal cancer. *Anticancer Res.* **2021**, *41*, 3589−3595.

(3) Brownstein, J.; Salama, J. K. Moderately hypofractionated proton beam therapy for locally advanced non-small cell lung cancer: a new way forward for dose escalation? *Int. J. Radiat. Oncol. Biol. Phys.* **2022**, *113*, 749−751.

(4) Polf, J. C.; Bronk, L. F.; Driessen, W. H.; Arap, W.; Pasqualini, R.; Gillin, M. Enhanced relative biological effectiveness of proton radiotherapy in tumor cells with internalized gold nanoparticles. *Appl. Phys. Lett.* **2011**, *98*, 193702.

(5) Qin, J.; Li, S.; Zhang, C.; Gao, D. W.; Li, Q.; Zhang, H.; Jin, X. D.; Liu, Y. Apoptosis and injuries of heavy ion beam and X-ray radiation on malignant melanoma cell. *Exp. Biol. Med.* **2017**, *242*, 953−960.

(6) Du, J.; Kageyama, S. I.; Hirata, H.; Motegi, A.; Nakamura, M.; Hirano, Y.; Okumura, M.; Yamashita, R.; Tsuchihara, K.; Hojo, H.; Hirayama, R.; Akimoto, T. Comparative analysis of the immune responses in cancer cells irradiated with X-ray, proton and carbon-ion beams. *Biochem. Biophys. Res. Commun.* **2021**, *585*, 55−60.

(7) Minatogawa, H.; Yasuda, K.; Dekura, Y.; Takao, S.; Matsuura, T.; Yoshimura, T.; Suzuki, R.; Yokota, I.; Fujima, N.; Onimaru, R.; Shimizu, S.; Aoyama, H.; Shirato, H. Potential benefits of adaptive intensity-modulated proton therapy in nasopharyngeal carcinomas. *J. Appl. Clin. Med. Phys.* **2021**, *22*, 174−183.

(8) Cunningham, L.; Penfold, S.; Giles, E.; Le, H.; Short, M. Impact of breast size on dosimetric indices in proton versus X-ray radiotherapy for breast cancer. *J. Pers. Med.* **2021**, *11*, 282.

(9) Britten, R. A.; Nazaryan, V.; Davis, L. K.; Klein, S. B.; Nichiporov, D.; Mendonca, M. S.; Wolanski, M.; Nie, X.; George, J.; Keppel, C. Variations in the RBE for cell killing along the depth-dose profile of a modulated proton therapy beam. *Radiat. Res.* **2013**, *179*, 21−28.

(10) Chaudhary, P.; Marshall, T. I.; Perozziello, F. M.; Manti, L.; Currell, F. J.; Hanton, F.; McMahon, S. J.; Kavanagh, J. N.; Cirrone, G. A.; Romano, F.; Prise, K. M.; Schettino, G. Relative biological effectiveness variation along monoenergetic and modulated Bragg peaks of a 62-MeV therapeutic proton beam: a preclinical assessment. *Int. J. Radiat. Oncol. Biol. Phys.* **2014**, *90*, 27−35.

(11) Paganetti, H. Relative biological effectiveness (RBE) values for proton beam therapy. Variations as a function of biological endpoint, dose, and linear energy transfer. *Phys. Med. Biol.* **2014**, *59*, R419−R472.

(12) Kwon, J.; Sutherland, K.; Hashimoto, T.; Shirato, H.; Date, H. Spatial distributions of dose enhancement around a gold nanoparticle at several depths of proton Bragg peak. *Nucl. Instrum. Methods Phys. Res. B* **2016**, *384*, 113−120.

(13) Cuaron, J. J.; Chang, C.; Lovelock, M.; Higginson, D. S.; Mah, D.; Cahlon, O.; Powell, S. Exponential increase in relative biological effectiveness along distal edge of a proton Bragg peak as measured by deoxyribonucleic acid double-strand breaks. *Int. J. Radiat. Oncol. Biol. Phys.* **2016**, *95*, 62−69.

(14) Seo, S. J.; Jeon, J. K.; Han, S. M.; Kim, J. K. Reactive oxygen species-based measurement of the dependence of the Coulomb nanoradiator effect on proton energy and atomic Z value. *Int. J. Radiat. Biol.* **2017**, *93*, 1239−1247.
(15) de Vera, P.; Abril, I.; Garcia-Molina, R. Energy spectra of protons and generated secondary electrons around the Bragg peak in materials of interest in proton therapy. *Radiat. Res.* **2018**, *190*, 282−297.
(16) Baumann, K. S.; Flatten, V.; Weber, U.; Lautenschläger, S.; Eberle, F.; Zink, K.; Engenhart-Cabillic, R. Effects of the Bragg peak degradation due to lung tissue in proton therapy of lung cancer patients. *Radiat. Oncol.* **2019**, *14*, 183.
(17) Byun, H. K.; Han, M. C.; Yang, K.; Kim, J. S.; Yoo, G. S.; Koom, W. S.; Kim, Y. B. Physical and biological characteristics of particle therapy for oncologists. *Cancer Res. Treat.* **2021**, *53*, 611−620.
(18) Berbeco, R. I.; Korideck, H.; Ngwa, W.; Kumar, R.; Patel, J.; Sridhar, S.; Johnson, S.; Price, B. D.; Kimmelman, A.; Makrigiorgos, G. M. DNA damage enhancement from gold nanoparticles for clinical MV photon beams. *Radiat. Res.* **2012**, *178*, 604−608.
(19) Oike, T.; Niimi, A.; Okonogi, N.; Murata, K.; Matsumura, A.; Noda, S. E.; Kobayashi, D.; Iwanaga, M.; Tsuchida, K.; Kanai, T.; Ohno, T.; Shibata, A.; Nakano, T. Visualization of complex DNA double-strand breaks in a tumor treated with carbon ion radiotherapy. *Sci. Rep.* **2016**, *6*, 22275.
(20) Schlathölter, T.; Lacombe, S.; Eustache, P.; Porcel, E.; Salado, D.; Stefancikova, L.; Tillement, O.; Lux, F.; Mowat, P.; van Goethem, M. J.; Remita, H.; Biegun, A. Improving proton therapy by metal-containing nanoparticles: nanoscale insights. *Int. J. Nanomed.* **2016**, *11*, 1549−1556.
(21) Abdul Rashid, R.; Zainal Abidin, S.; Khairil Anuar, M. A.; Tominaga, T.; Akasaka, H.; Sasaki, R.; Kie, K.; Abdul Razak, K.; Pham, B. T. T.; Hawkett, B. S.; Carmichael, M. A.; Geso, M.; Rahman, W. N. Radiosensitization effects and ROS generation by high Z metallic nanoparticles on human colon carcinoma cell (HCT116) irradiated under 150 MeV proton beam. *Open Nano* **2019**, *4*, 100027.
(22) Suckert, T.; Müller, J.; Beyreuther, E.; Azadegan, B.; Brüggemann, A.; Bütof, R.; Dietrich, A.; Gotz, M.; Haase, R.; Schürer, M.; Tillner, F.; von Neubeck, C.; Krause, M.; Lühr, A. High-precision image-guided proton irradiation of mouse brain sub-volumes. *Radiother. Oncol.* **2020**, *146*, 205−212.
(23) Horendeck, D.; Walsh, K. D.; Hirakawa, H.; Fujimori, A.; Kitamura, H.; Kato, T. A. High LET-like radiation tracks at the distal side of accelerated proton Bragg peak. *Front. Oncol.* **2021**, *11*, 690042.
(24) Frame, C. M.; Chen, Y.; Gagnon, J.; Yuan, Y.; Ma, T.; Dritschilo, A.; Pang, D. Proton induced DNA double strand breaks at the Bragg peak: evidence of enhanced LET effect. *Front. Oncol.* **2022**, *12*, 930393.
(25) Marshall, T. I.; Chaudhary, P.; Michaelidesová, A.; Vachelová, J.; Davídková, M.; Vondráček, V.; Schettino, G.; Prise, K. M. Investigating the implications of a variable RBE on proton dose fractionation across a clinical pencil beam scanned spread-out Bragg peak. *Int. J. Radiat. Oncol. Biol. Phys.* **2016**, *95*, 70−77.
(26) Tao, L.; Zhu, K.; Zhu, J.; Xu, X.; Lin, C.; Ma, W.; Lu, H.; Zhao, Y.; Lu, Y.; Chen, J. E.; Yan, X. An analytical reconstruction model of the spread-out Bragg peak using laser-accelerated proton beams. *Phys. Med. Biol.* **2017**, *62*, 5200−5212.
(27) Hojo, H.; Dohmae, T.; Hotta, K.; Kohno, R.; Motegi, A.; Yagishita, A.; Makinoshima, H.; Tsuchihara, K.; Akimoto, T. Difference in the relative biological effectiveness and DNA damage repair processes in response to proton beam therapy according to the positions of the spread out Bragg peak. *Radiat. Oncol.* **2017**, *12*, 111.
(28) Ghorbani, M.; Jia, S. B.; Khosroabadi, M.; Sadoughi, H. R.; Knaup, C. Evaluation of the effect of soft tissue composition on the characteristics of spread-out Bragg peak in proton therapy. *J. Cancer Res. Ther.* **2017**, *13*, 974−980.
(29) Malmir, S.; Mowlavi, A. A.; Mohammadi, S. Enhancement evaluation of energy deposition and secondary particle production in gold nanoparticle aided tumor using proton therapy. *Int. J. Cancer Manag.* **2017**, *10*, No. e10719.
(30) Grün, R.; Friedrich, T.; Krämer, M.; Scholz, M. Systematics of relative biological effectiveness measurements for proton radiation along the spread out Bragg peak: experimental validation of the local effect model. *Phys. Med. Biol.* **2017**, *62*, 890−908.
(31) Hawkins, R. B. Biological effective dose for treatment of a heterogeneous population of cells with a spread-out Bragg peak of particle radiation. *Radiat. Res.* **2021**, *196*, 386−393.
(32) Chithrani, D. B.; Jelveh, S.; Jalali, F.; van Prooijen, M.; Allen, C.; Bristow, R. G.; Hill, R. P.; Jaffray, D. A. Gold nanoparticles as radiation sensitizers in cancer therapy. *Radiat. Res.* **2010**, *173*, 719−728.
(33) Kim, J. K.; Seo, S. J.; Kim, K. H.; Kim, T. J.; Chung, M. H.; Kim, K. R.; Yang, T. K. Therapeutic application of metallic nanoparticles combined with particle-induced x-ray emission effect. *Nanotechnology* **2010**, *21*, 425102.
(34) Jain, S.; Coulter, J. A.; Hounsell, A. R.; Butterworth, K. T.; McMahon, S. J.; Hyland, W. B.; Muir, M. F.; Dickson, G. R.; Prise, K. M.; Currell, F. J.; et al. Cell-specific radiosensitization by gold nanoparticles at megavoltage radiation energies. *Int. J. Radiat. Oncol. Biol. Phys.* **2011**, *79*, 531−539.
(35) Jeremic, B.; Aguerri, A. R.; Filipovic, N. Radiosensitization by gold nanoparticles. *Clin. Transl. Oncol.* **2013**, *15*, 593−601.
(36) Jeynes, J. C.; Merchant, M. J.; Spindler, A.; Wera, A. C.; Kirkby, K. J. Investigation of gold nanoparticle radiosensitization mechanisms using a free radical scavenger and protons of different energies. *Phys. Med. Biol.* **2014**, *59*, 6431−6443.
(37) Retif, P.; Pinel, S.; Toussaint, M.; Frochot, C.; Chouikrat, R.; Bastogne, T.; Barberi-Heyob, M. Nanoparticles for radiation therapy enhancement: the key parameters. *Theranostics* **2015**, *5*, 1030−1044.
(38) Chen, N.; Yang, W.; Bao, Y.; Xu, H.; Qin, S.; Tu, Y. BSA capped Au nanoparticle as an efficient sensitizer for glioblastoma tumor radiation therapy. *RSC Adv.* **2015**, *5*, 40514−40520.
(39) Lin, Y.; Held, K.; McMahon, S.; Paganetti, H.; Schuemann, J. SU-E-T-518: Investigation of Gold Nanoparticle Radiosensitization for Carbon Ion Therapy. *Med. Phys.* **2015**, *42*, 3454.
(40) Lin, Y.; McMahon, S. J.; Paganetti, H.; Schuemann, J. Biological modeling of gold nanoparticle enhanced radiotherapy for proton therapy. *Phys. Med. Biol.* **2015**, *60*, 4149−4168.
(41) Enferadi, M.; Fu, S. Y.; Hong, J. H.; Tung, C. J.; Chao, T. C.; Wey, S. P.; Chiu, C. H.; Wang, C. C.; Sadeghi, M. Radiosensitization of ultrasmall GNP-PEG-cRGDfK in ALTS1C1 exposed to therapeutic protons and kilovoltage and megavoltage photons. *Int. J. Radiat. Biol.* **2018**, *94*, 124−136.
(42) Cunningham, C.; de Kock, M.; Engelbrecht, M.; Miles, X.; Slabbert, J.; Vandevoorde, C. Radiosensitization effect of gold nanoparticles in proton therapy. *Front. Public Health* **2021**, *9*, 699822.
(43) Hawkins, R. B. Biological effective dose for treatment of a heterogeneous population of cells with a spread-out Bragg peak of particle radiation. *Radiat. Res.* **2021**, *196*, 386−393.
(44) McMahon, S. J.; Hyland, W. B.; Muir, M. F.; Coulter, J. A.; Jain, S.; Butterworth, K. T.; Schettino, G.; Dickson, G. R.; Hounsell, A. R.; O'Sullivan, J. M.; Prise, K. M.; Hirst, D. G.; Currell, F. J. Biological consequences of nanoscale energy deposition near irradiated heavy atom nanoparticles. *Sci. Rep.* **2011**, *1*, 18.
(45) Wolfe, T.; Guidelli, E. J.; Gómez, J. A.; Baffa, O.; Nicolucci, P. Experimental assessment of gold nanoparticle-mediated dose enhancement in radiation therapy beams using electron spin resonance dosimetry. *Phys. Med. Biol.* **2015**, *60*, 4465−4480.
(46) Kwon, J.; Sutherland, K.; Hashimoto, T.; Date, H. Dose distribution of electrons from gold nanoparticles by proton beam irradiation. *Int. J. Med. Phys. Clin. Eng. Radiat. Oncol.* **2015**, *04*, 49−53.
(47) Van Houten, B.; Woshner, V.; Santos, J. H. Role of mitochondrial DNA in toxic responses to oxidative stress. *DNA Repair* **2006**, *5*, 145−152.
(48) Alan Mitteer, R.; Wang, Y.; Shah, J.; Gordon, S.; Fager, M.; Butter, P. P.; Jun Kim, H.; Guardiola-Salmeron, C.; Carabe-Fernandez, A.; Fan, Y. Proton beam radiation induces DNA damage

https://doi.org/10.1021/acsomega.3c01025
ACS Omega 2023, 8, 17922−17931

and cell apoptosis in glioma stem cells through reactive oxygen species. *Sci. Rep.* **2015**, *5*, 13961.
(49) Kim, J. K.; Seo, S. J.; Kim, H. T.; Kim, K. H.; Chung, M. H.; Kim, K. R.; Ye, S. J. Enhanced proton treatment in mouse tumors through proton irradiated nanoradiator effects on metallic nanoparticles. *Phys. Med. Biol.* **2012**, *57*, 8309−8323.
(50) Chow, J. C.; Leung, M. K.; Jaffray, D. A. Monte Carlo simulation on a gold nanoparticle irradiated by electron beams. *Phys. Med. Biol.* **2012**, *57*, 3323−3331.
(51) Douglass, M.; Bezak, E.; Penfold, S. Monte Carlo investigation of the increased radiation deposition due to gold nanoparticles using kilovoltage and megavoltage photons in a 3D randomized cell model. *Med. Phys.* **2013**, *40*, 071710.
(52) Tsiamas, P.; Liu, B.; Cifter, F.; Ngwa, W. F.; Berbeco, R. I.; Kappas, C.; Theodorou, K.; Marcus, K.; Makrigiorgos, MG.; Sajo, E.; Zygmanski, P. Impact of beam quality on megavoltage radiotherapy treatment techniques utilizing gold nanoparticles for dose enhancement. *Phys. Med. Biol.* **2013**, *58*, 451−464.
(53) Lechtman, E.; Mashouf, S.; Chattopadhyay, N.; Keller, B. M.; Lai, P.; Cai, Z.; Reilly, R. M.; Pignol, J. P. A Monte Carlo-based model of gold nanoparticle radiosensitization accounting for increased radiobiological effectiveness. *Phys. Med. Biol.* **2013**, *58*, 3075−3087.
(54) Newpower, M.; Ahmad, S.; Chen, Y. SU-E-J-247: A Simulation of X-Ray Emission with Gold Nanoparticle Irradiated by Energetic Proton Beam. *Med. Phys.* **2014**, *41*, 214−215.
(55) Lin, Y.; McMahon, S. J.; Scarpelli, M.; Paganetti, H.; Schuemann, J. Comparing gold nano-particle enhanced radiotherapy with protons, megavoltage photons and kilovoltage photons: A Monte Carlo simulation. *Phys. Med. Biol.* **2014**, *59*, 7675−7689.
(56) Wälzlein, C.; Scifoni, E.; Krämer, M.; Durante, M. Simulations of dose enhancement for heavy atom nanoparticles irradiated by protons. *Phys. Med. Biol.* **2014**, *59*, 1441−1458.
(57) Gao, J.; Zheng, Y. Monte Carlo study of secondary electron production from gold nanoparticle in proton beam irradiation. *Int. J. Cancer Ther. Oncol.* **2014**, *2*, 02025.
(58) Kirkby, C.; Ghasroddashti, E. Targeting mitochondria in cancer cells using gold nanoparticle-enhanced radiotherapy: A Monte Carlo study. *Med. Phys.* **2015**, *42*, 1119−1128.
(59) Peukert, D.; Kempson, I.; Douglass, M.; Bezak, E. Gold nanoparticle enhanced proton therapy: Monte Carlo modeling of reactive species' distributions around a gold nanoparticle and the effects of nanoparticle proximity and clustering. *Int. J. Mol. Sci.* **2019**, *20*, 4280.
(60) Peukert, D.; Kempson, I.; Douglass, M.; Bezak, E. Gold nanoparticle enhanced proton therapy: A Monte Carlo simulation of the effects of proton energy, nanoparticle size, coating material, and coating thickness on dose and radiolysis yield. *Med. Phys.* **2020**, *47*, 651−661.
(61) Rajabpour, S.; Saberi, H.; Rasouli, J.; Jabbari, N. Comparing Geant4 physics models for proton-induced dose deposition and radiolysis enhancement from a gold nanoparticle. *Sci. Rep.* **2022**, *12*, 1779.
(62) Sotiropoulos, M.; Henthorn, N. T.; Warmenhoven, J. W.; Mackay, R. I.; Kirkby, K. J.; Merchant, M. J. Modelling direct DNA damage for gold nanoparticle enhanced proton therapy. *Nanoscale* **2017**, *9*, 18413−18422.
(63) Taggart, L. E.; McMahon, S. J.; Currell, F. J.; Prise, K. M.; Butterworth, K. T. The role of mitochondrial function in gold nanoparticle mediated radiosensitisation. *Cancer Nano* **2014**, *5*, 5.
(64) Howard, D.; Sebastian, S.; Le, Q. V. C.; Thierry, B.; Kempson, I. Chemical mechanisms of nanoparticle radiosensitization and radioprotection: a review of structure-function relationships influencing reactive oxygen species. *Int. J. Mol. Sci.* **2020**, *21*, 579.
(65) Liaw, J. W.; Kuo, C. Y.; Tsai, S. W. The effect of quasi-spherical gold nanoparticles on two-photon induced reactive oxygen species for cell damage. *Nanomaterials* **2021**, *11*, 1180.
(66) Tsai, S. W.; Lo, C. Y.; Yu, S. Y.; Chen, F. H.; Huang, H. C.; Wang, L. K.; Liaw, J. W. Gold nanoparticles enhancing generation of ROS for Cs-137 radiotherapy. *Nanoscale Res. Lett.* **2022**, *17*, 123.
(67) Li, S.; Penninckx, S.; Karmani, L.; Heuskin, A. C.; Watillon, K.; Marega, R.; Zola, J.; Corvaglia, V.; Genard, G.; Gallez, B.; et al. LET-dependent radiosensitization effects of gold nanoparticles for proton irradiation. *Nanotechnology* **2016**, *27*, 455101.
(68) Li, S.; Bouchy, S.; Penninckx, S.; Marega, R.; Fichera, O.; Gallez, B.; Feron, O.; Martinive, P.; Heuskin, A. C.; Michiels, C.; Lucas, S. Antibody-functionalized gold nanoparticles as tumor targeting radiosensitizers for proton therapy. *Nanomedicine* **2019**, *14*, 317−333.
(69) Lacombe, S.; Porcel, E.; Scifoni, E. Particle therapy and nanomedicine: state of art and research perspectives. *Cancer Nanotechnol.* **2017**, *8*, 9.
(70) Penninckx, S.; Heuskin, A. C.; Michiels, C.; Lucas, S. Gold nanoparticles as a potent radiosensitizer: a transdisciplinary approach from physics to patient. *Cancers* **2020**, *12*, 2021.

https://doi.org/10.1021/acsomega.3c01025
ACS Omega 2023, 8, 17922−17931